Plasmon-Enhanced Fluorescence-Based Core–Shell Gold Nanorods as a Near-IR Fluorescent Turn-On Sensor for the Highly Sensitive Detection of Pyrophosphate in Aqueous Solution

*Le Wang, Quanwei Song, Qiuling Liu, Dacheng He, and Jin Ouyang**

Developing plasmon-enhanced fluorescence (PEF) technology for identifying important biological molecules has a profound impact on biosensing and bioimaging. However, exploration of PEF for biological application is still at a very early stage. Herein, novel PEF-based core–shell nanostructures as a near-infrared fluorescent turn-on sensor for highly sensitive and selective detection of pyrophosphate (PPi) in aqueous solution are proposed. This nanostructure gold nanorod (AuNR)@SiO_2@*meso*-tetra(4-carboxyphenyl) porphyrin (TCPP) contains a gold nanorod core with an aspect ratio of 2.3, a silica shell, and TCPP molecules covalently immobilized onto the shell surface. The silica shell is employed a rigid spacer for precisely tuning the distance between AuNR and TCPP and an optimum fluorescence enhancement is obtained. Due to the quenching effect of Cu^{2+}, the copper porphyrin (TCPP-Cu^{2+}) results in a weak fluorescence. In the presence of PPi, the strong affinity between Cu^{2+} and PPi can promote the disassembly of the turn-off state of TCPP-Cu^{2+} complexes, and therefore the fluorescence can be readily restored. By virtue of the amplified fluorescence signal imparted by PEF, this nanosensor obtains a detection limit of 820×10^{-9} M of PPi with a good selectivity over several anions, including phosphate. Additionally, the potential applicability of this sensor in cell imaging is successfully demonstrated.

1. Introduction

Great efforts have been devoted to developing rapid and cost-effective fluorescence technique for identifying and observing biological molecules and therefore strategies that improve biomolecular detection would have a profound impact on a variety of biomedical and biological applications, such as biosensing, cell imaging, and high-throughput diagnostics.[1] Thus, plasmon-enhanced fluorescence (PEF)[2,3] becomes an emerging technology by virtue of its capability to largely amplify fluorescence signals and significantly improve the detection sensitivity.[4,5] When the excited-state fluorophores are located in close proximity to metal nanomaterials, the fluorescence intensity can be strongly enhanced by the interactions of intense plasmon-induced electric fields.[6–10] More importantly, it has been proved that PEF gives rise to enhancement of quantum yield, reduction of fluorescence lifetime, as well as improvement of photostability, which shed some light on addressing the drawbacks of the majority of fluorescent molecules, especially for near-infrared (NIR) dyes, paving the way for its application in biosensors.[11,12] Numerous factors, including nanoparticles (NPs) geometry, size, the quantum yields of fluorophores, and the gap distance between fluorophores and metal nanostructure surface, are responsible for PEF. Recently, aspherical nanomaterials such as rods[13] and triangles,[14] are of great interest owing to their larger scattering cross section and spatial focus of the near field of the localized surface plasmon resonance (LSPR).[15] Compared with spherical metal nanomaterials, gold nanorods (AuNRs) with rod-like shapes exhibit many excellent advantages such as tunable shape and size, functionalization hybrid structures, anisotropic electronic, optical and plasmonic properties, which are favorable to cause stronger plasmon resonance.[16] Some groups have put the fluorophores in interaction with lithographically fabricated anisotropic nanostructures for the achievement of PEF.[2,17] However, this lithographically method for enhancing the fluorescence has a number of shortcomings compared with colloidal approaches. 1) Lithography has the ability to support the fabrication of 2D nanostructures rather than 3D structures with controllable gaps and geometries in large scale, and the prepared metal nanostructures are difficult and expensive.[4] 2) The nonmotile metal film is not suitable for probing the contents of samples in biosensing and cell imaging applications.[18] Notably, the solution–PEF system is more appropriate for applications in biological systems. Unfortunately, PEF is

L. Wang, Dr. Q. Song, Q. Liu, Prof. J. Ouyang
Key Laboratory of Theoretical and Computational Photochemistry
Ministry of Education
College of Chemistry
Beijing Normal University
Beijing 100875, P. R. China
E-mail: jinoyang@bnu.edu.cn
Prof. D. He
Key Laboratory of Cell Proliferation and Regulation Biology
Ministry of Education
Beijing Normal University
Beijing 100875, P. R. China

DOI: 10.1002/adfm.201503326

rarely observed in bulk solution. Thus, the fabrication of universal PEF nanostructures (especially AuNRs) and the development of their solution-based biosensing applications would be desirable.

From investigation by recent theoretical and experimental studies,[4,19–22] the strong PEF effect is ascribed to the specific fluorescent molecule with its absorption and emission close to the surface plasmon resonance of metal nanostructures by avoiding nonradiative energy transfer and offering a stronger electromagnetic field. Notably, Singamaneni groups[2] recently reported that the fluorescence intensity of NIR dyes that are precisely place in proximity to AuNR can be significantly improved by adjusting the dielectric spacers for precisely tuning the distance between AuNR and NIR dyes as well as LSPR wavelength, further confirming that the distance dependence plays a key role in the fluorescence enhancement. However, these adsorption methods for achieving PEF effect is difficult to be extensively used, especially for biosensing, as desorption effects of the absorbed dyes can inevitably cause strong background interference. Core–shell structures, such as the silica matrix as a shell around the metallic core,[23] provide access to the ease of surface chemical modification, which may efficiently overcome the difficulty mentioned above. Silica coating AuNR (AuNR@SiO_2) can not only improve the stability and biocompatibility of metal nanostructures[24,25] but also offer a tunable rigid spacer to control the gap distance for optimizing the fluorescence efficiency.[26] In addition, through covalently linking fluorescence molecules to metal nanostructures surface, their fluorescence performance as imaging probes or photosensitizers theoretically and experimentally can be improved.[27,28] Hence, the creation of universal PEF-based core–shell AuNR@SiO_2 as sensors or probes would be beneficial for the development of diagnostics and clinical applications.

Pyrophosphate (PPi) as a kind of important biofunctional anions involves in energy transduction in organisms and several metabolic processes, which becomes one of the most popular targets for recognition studies.[29,30] As the byproduct of cellular hydrolysis of adenosine triphosphate (ATP), PPi is closely related to the process of the replication of DNA and the expression of genetic information, and thus the detection of PPi has been recognized as a kind of real-time DNA sequencing method. The intracellular PPi concentrations can be used to describe the levels of DNA replication, which has become an important indicator in cancer diagnosis.[31] The abnormal PPi concentrations can help identifying vascular calcification such as calcium pyrophosphate dihydrate (CPPD) crystal deposition disease.[32] Given the significance of PPi, numerous PPi reactive and selective fluorescent probes have been developed in the past decades.[33–35] However, owing to the issues, including strong hydration of anions and low solubility of organic probes, the majority of methods require organic or mixed aqueous media in previous researches, which greatly limits analytical application.[36,37] Up to now, the sensitivity toward PPi detection in aqueous media is invariably limited to micromolar levels in recent reports[38,39] and their emission spectra are mostly in the short wavelength range from 400 to 600 nm. NIR (650–900 nm)[40] fluorescent probe attracts more attention with unique advantages, such as deep tissue penetration, lower damage of biological samples, and minimal autofluorescence with much lower background interference. However, the majority of existing NIR fluorophores exhibit low quantum yield, which limits their progress in clinical applications. Considering that the PEF strategy can improve the optical properties of NIR fluorophores,[2] it is of great significance to develop NIR sensors based on PEF nanostructures for highly sensitive and selective PPi detection in 100% aqueous solution.

The formed dye–metal complexes through meta–ligand interaction can serve as a classical kind of organic fluorescent sensor for sensitive and selective turn-on sensing of PPi.[29] Inspired by the displacement strategies, herein we first present the design and synthesis of an organic–inorganic hybrid sensor system using PEF-based core–shell nanostructures (AuNR@SiO_2@*meso*-tetra(4-carboxyphenyl) porphyrin (TCPP)) that consist of AuNR core, controllable silica shell, and molecule layer of porphyrin (**Scheme 1**A). TCPP as fluorescence emitter is covalently attached to the AuNR surface with controllable silica shell thickness, resulting in the significant enhancement of fluorescence intensity via plasmon–exciton coupling. Cu^{2+} is a well-known highly efficient fluorescent quencher due to its paramagnetic properties via electron or energy transfer, and as a result the copper porphyrin (TCPP-Cu^{2+}) has a weak fluorescence.[41] Upon the introduction of PPi, the strong affinity between Cu^{2+} and PPi can promote the disassembly of the turn-off state of TCPP-Cu^{2+} complexes,[42,43] and the process can be observed by monitoring the fluorescence recovery of TCPP (Scheme 1B). In addition, no obvious change in fluorescence intensity would be expected for other interferences from analogues of PPi as well as others, because the formed complex of Cu^{2+} and PPi through coordination could be more stable than others.[38,44] Accordingly, an NIR fluorescent turn-on sensing approach for sensitive and selective PPi detection can be established. To the best knowledge, this is the first example of PEF-based nanostructures for sensing PPi in 100% aqueous solution. Owing to the signal amplification, this sensor responds toward PPi even at nanomolar concentrations with high selectivity over many inorganic anions. Given the good biocompatibility of AuNR@SiO_2@TCPP, the potential application of this novel PEF-based fluorescent probe is demonstrated by fluorescent imaging of PPi in living cells.

2. Results and Discussion

2.1. Characterization and PEF Performance of AuNR@SiO_2@TCPP

The morphology of prepared AuNRs and AuNR@SiO_2 NPs was determined by high-resolution transmission electron microscopy (HR-TEM). As shown in **Figure 1**A, AuNRs showed an average length of 49 ± 5 nm, a diameter of 21 ± 3 nm with an aspect ratio of ≈2.3. AuNRs were synthesized using a seeding growth method and stabilized by the cetyltrimethylammonium bromide (CTAB) to form CTAB-coated AuNRs. The claviform AuNRs had two ends and an anisotropic structure, which may facilitate a preferred PEF effect. Figure 1B showed the AuNRs were coated with silica shell and the silica shell thickness could be tuned by changing the concentration of CTAB mentioned

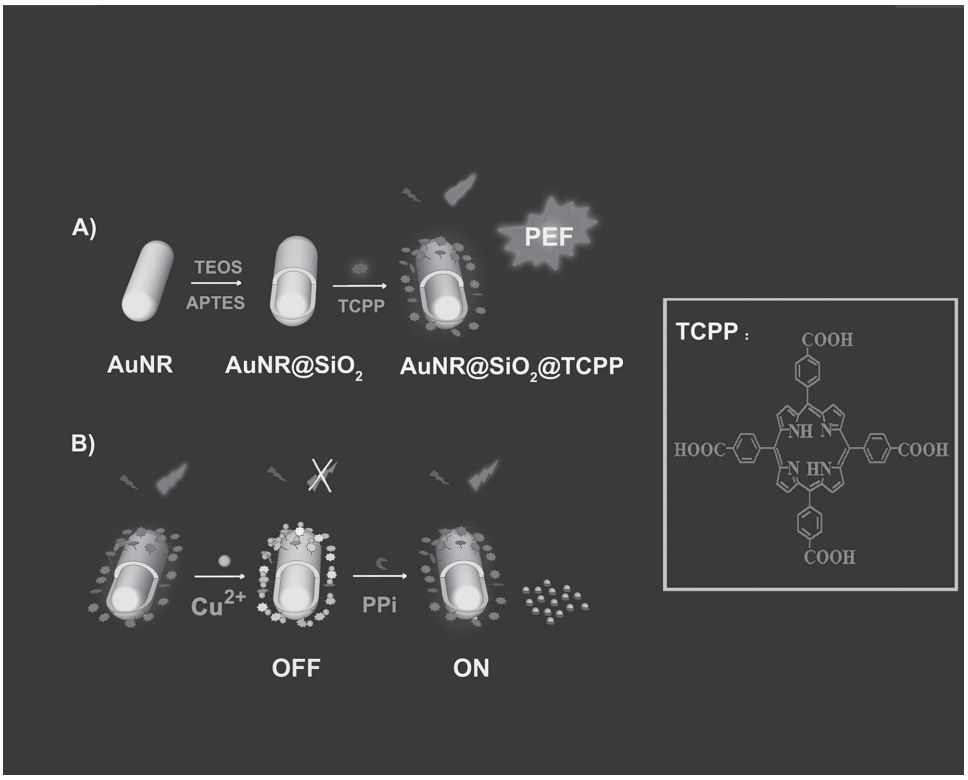

Scheme 1. A) Schematic illustration of the preparation of PEF-based core–shell AuNR@SiO_2@TCPP NPs. B) Schematic illustration of the designed PEF-based core–shell AuNR@SiO_2@TCPP NPs as fluorescence probes for the detection of PPi.

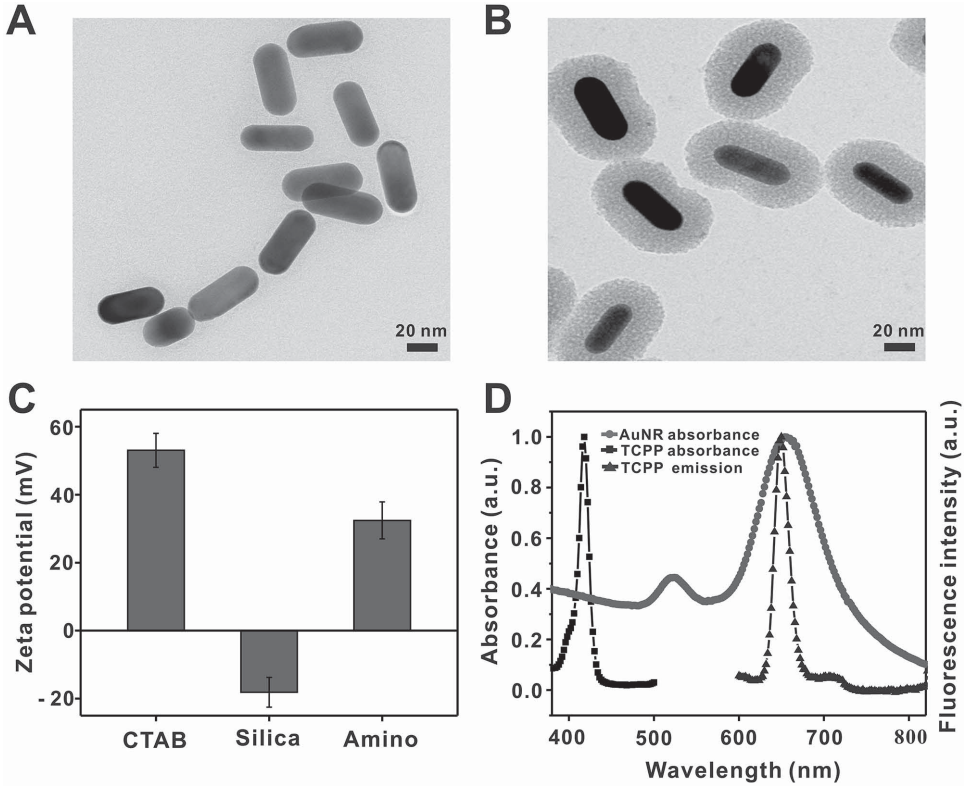

Figure 1. A) TEM images of the prepared AuNRs. B) TEM images of the prepared core–shell AuNR@SiO_2. C) Zeta-potential values of AuNRs coated with CTAB, silica shell, and functionalized with the amino. D) UV–vis spectra of AuNRs, absorbance, and fluorescence spectra of TCPP.

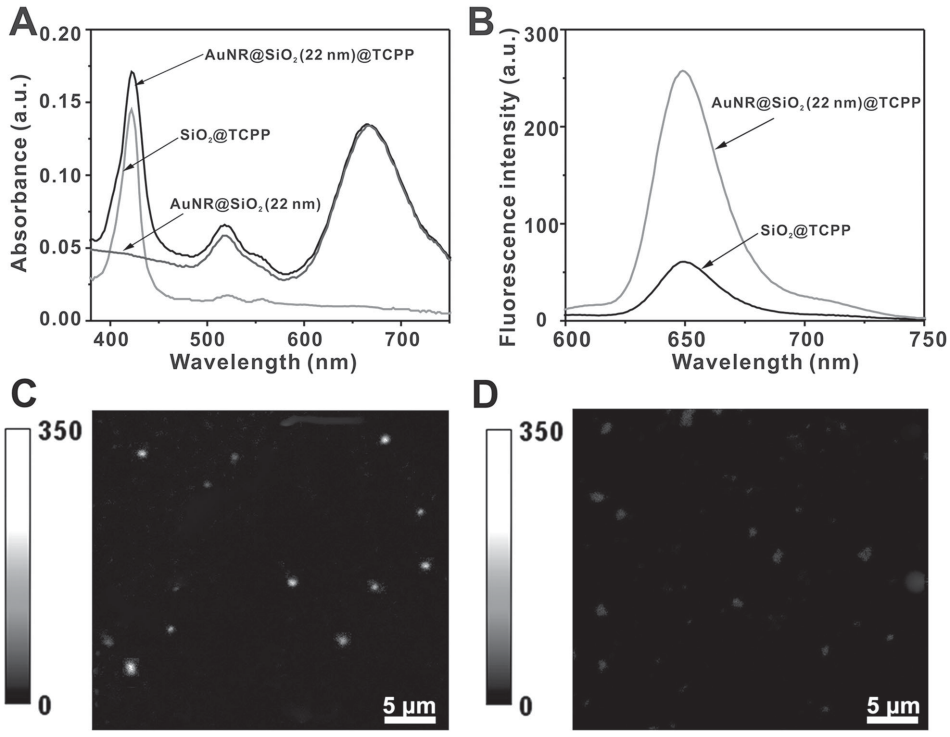

Figure 2. A) UV–vis spectra of AuNR@SiO_2 (22 nm)@TCPP, SiO_2@TCPP, and AuNR@SiO_2 (22 nm). B) Fluorescence spectra of the control sample SiO_2@TCPP and AuNR@SiO_2 (22 nm)@TCPP NPs with a silica shell thickness of 22 nm. C) A confocal scanning fluorescence image of AuNR@SiO_2 (22 nm)@TCPP NPs. D) A confocal scanning fluorescence image of the control sample SiO_2@TCPP.

in the AuNR@SiO_2 NPs preparation section. The silica-coated AuNR@SiO_2 NPs were then functionalized $-NH_2$ groups by introducing 3-aminopropyltrime-thoxysilane (APTES) (a silane coupling agent). This functionalization of AuNRs could be checked by the measurement of Zeta potential (Figure 1C). The as-synthesized AuNRs carried a positive charge because of protecting by CTAB. After silica coating and purification, the surface charge was negative because of surface silanol groups. Upon amino functionalization, the surface charge of the nanorods approached positive, confirming the successful functionalization of amino on the silica surface. Considering that porphyrins were a kind of hydrosoluble and modified macrocyclic compounds, we choose a well-known commercially available TCPP as a model molecule for proof-of-concept experiments. The molecular structure of TCPP (Scheme 1) contained carbonyl groups that enabled TCPP covalently linking to the silica shell via formation of a stable amide bond using *N*-(3-dimethyl-aminopropyl)-*N*-ethylcarbodiimide hydrochloride (EDC) and *N*-hydroxysuccinimide (NHS).[27,45] This conjugation method made a promise to incorporation of any amine-reactive dyes onto the silica shell to load a plenty of fluorophores or biomolecules. Thus, appropriate AuNR@SiO_2@TCPP NPs were successfully synthesized, and the silica between AuNRs and TCPP was well controlled with relatively high uniformity.

Recently, many studies have been devoted to the interactions between fluorophores and the plasmon resonances.[46,47] It has been proved that the fluorescence enhancement would be optimal when there was stronger spectral overlap between the plasmon band of NPs and emission spectrum of the fluorophores.[4,7,8,21] As shown in Figure 1D, the normalized UV–vis absorption spectra of the AuNRs suspension exhibited the longitudinal plasmon peak at 654 nm, which was in close resonance with TCPP ($\lambda_{max,abs}$ = 419 nm, $\lambda_{max,em}$ = 650 nm). In order to evaluate the PEF of AuNRs, the fluorescence intensity of SiO_2@TCPP as the control sample was carried out under the same chemical environment in all measurements. The prepared SiO_2@TCPP NPs were quite monodisperse with an averaged diameter of 50 ± 6 nm (Figure S1, Supporting Information). According to previous reports,[27,46,48] it was reasonable to choose SiO_2@TCPP as the reference because fluorescence lifetime and steady-state fluorescence intensity of SiO_2@TCPP behaved similar to free TCPP. These results indicated that simply binding TCPP to the silica surface did not significantly change fluorescence behavior, but ensured identical environment as much as possible. As shown in **Figure 2**A, AuNR@SiO_2@TCPP NPs with silica shell thickness of 22 nm (AuNR@SiO_2 (22 nm)@TCPP) have two strong SPR bands of AuNRs as well as an extra absorption band peaking at 419 nm owing to the conjugation of TCPP molecules. The amount of TCPP molecules covalently linked to silica shell could be calculated through the absorption spectra. The relative ratio of TCPP to AuNR@SiO_2 was roughly estimated to be about 4200 TCPP molecules per AuNR@SiO_2 by using the reported method[27,49] (Section S2, Supporting Information). The total concentration of TCPP in AuNR@SiO_2@TCPP NPs should be almost the same as that in SiO_2@TCPP. Meanwhile, an obvious fluorescence enhancement process was observed (Figure 2B), and the fluorescence intensity could increase up to ≈4.5 times by

0.09×10^{-9} M AuNR@SiO_2@TCPP at a silica thickness of 22 nm. It matched very well with previous reports that PEF was strongly separation distance dependent.[2,27,46] Typical confocal scanning images with a size of 35 μm × 35 μm were taken from AuNR@SiO_2@TCPP with 22 nm silica shell (Figure 2C) and the control sample SiO_2@TCPP (Figure 2D). The prominent differences in brightness of emission spots indicated unambiguous information of fluorescence enhancement in the presence of AuNRs. The fluorescence intensity of AuNR@SiO_2@TCPP was ≈4.5-fold higher than that of the control sample. This showed that AuNR core was responsible for fluorescence emission enhancement, which was attributed to the PEF phenomenon.

2.2. Optimization and Mechanism of PEF for AuNR@SiO_2@TCPP

The fluorescence enhancement was closely related to the distance between the fluorophores and the metal NPs. Although there were a few attempts to use protein[47] or polyelectrolyte[50] to control the distance, a rigid dielectric spacer layer was more advantageous to accurately regulate the spacer thickness and investigate the mechanism. In order to get the optimized fluorescence enhancement ability, the silica thickness was controlled by CTAB concentration.[46] The key process was adjusting the concentration of CTAB less than 0.01×10^{-3} M by centrifugation twice after prepared. Extra centrifugation was not required because total CTAB removal from the surface caused AuNRs aggregation. In the silica coating procedures, concentration of CTAB was varied between 0.3 and 1.8×10^{-3} M to obtain porous shell thickness about 34, 28, 22, 18, 13, and 8 nm (**Figure 3**A–F). The concentration of CTAB versus the used silica shell thickness was shown in Figure S3 (Supporting Information). It demonstrated that silica shell thickness decreased while the CTAB concentration increased. As shown in Figure S4 (Supporting Information), the absorption spectra of AuNR@SiO_2 had a red shift compared with the bare AuNR, which was induced by the increase in the local refractive index of the silica shell and the decreased plasmon oscillation energy.[51]

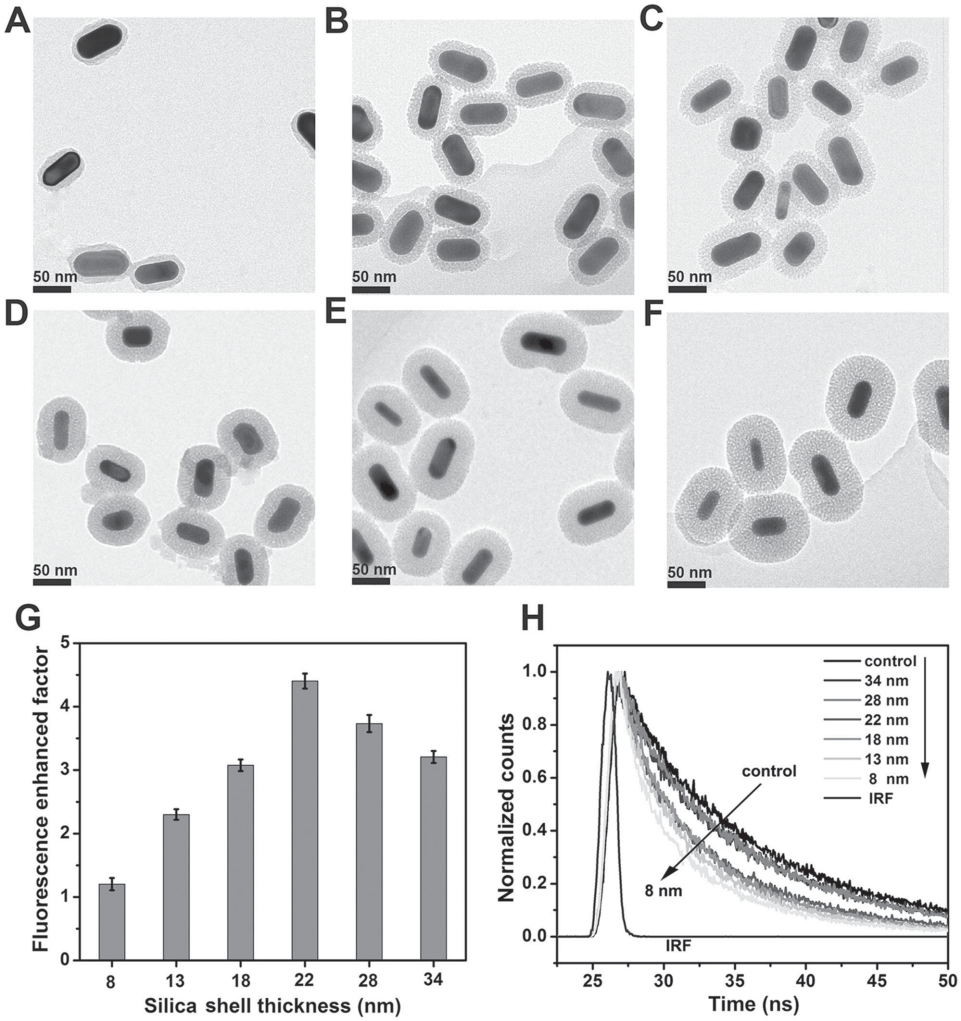

Figure 3. A–F) TEM images of AuNR@SiO_2 with increasing silica shell thickness (8, 13, 18, 22, 28, and 34 nm). G) Distance-dependent fluorescence enhancement factor. H) Fluorescence decay curves of AuNR@SiO_2@TCPP with different silica shell thickness (8, 13, 18, 22, 28, and 34 nm) and the control sample.

At a distance of a few nanometers from the metal surface, the fluorescence was strongly enhanced, which was reported by increasing studies.[12,18,47,52] Accordingly, we tested a series of AuNR@SiO_2 with above-mentioned shell thickness from 8 to 34 nm in order to study the distance-dependent enhancement effect for the optimized fluorescence enhancement ability. The fluorescence enhancement was characterized using fluorescence enhancement factor F ($F = I/I_{control}$, where I was the emission intensity of PEF-AuNR@SiO_2@TCPP and $I_{control}$ was the emission intensity of SiO_2@TCPP). The result showed in Figure 3G, for our PEF system, the largest fluorescence enhancement was observed at a silica shell thickness of 22 nm with enhancement factor of 4.5. Thicker shell thickness resulted in decreased fluorescence enhancement and thinner shell thickness caused less fluorescence enhancement (Figure S5, Supporting Information). Thus, AuNR@SiO_2@TCPP with the silica shell thickness of 22 nm was used for the following detection.

To explore the origin of PEF, the fluorescence decay curves of TCPP in SiO_2@TCPP and AuNR@SiO_2@TCPP NPs with different shell thickness were observed by time-correlated single photon counting (TCSPC) technique (Figure 3H). All of the fluorescence of AuNR@SiO_2@TCPP decayed much faster than that on SiO_2 (SiO_2@TCPP), leading to shortened fluorescence lifetimes (Table S1, Supporting Information), which suggested that the shortened lifetime arose from the interaction of the fluorophore and AuNR core through modification of decay rate.[12,53] The fluorescence enhancement mechanism by the interactions between plasmons and fluorophores has been widely studied lately.[54] There were two kinds of enhancement contributions:[21,55,56] excitation enhancement owing to strong local electric fields associated with the excitation of localized surface plasmon resonance and increase in the radiative decay rate from a surface plasmon resonance-coupled excited state of the fluorophore. Excitation enhancement which depended on the plasmon resonance overlap with the excitation wavelength, resulted in an enhanced local electric field due to plasmon resonance increased the rate of excitation but did not change the fluorescence lifetime.[22] The increase of radiative decay rate could lead to decreased fluorescence lifetime and increased fluorescence quantum yields (i.e., fluorescence intensity) because of an increase in intrinsic radiative decay rate of the fluorophore,[12,18] which was consistent with our experimental observation due to spectral overlap between the plasmon band of AuNRs and emission spectrum of TCPP.

As Lakowicz and co-workers reported,[12,57] as the value of metal increased radiative rate increased, the fluorescence quantum yield increased while the lifetime tended to decrease. In our experimental results, no fluorescence quenching was observed, indicating that the radiative decay rate always took the dominant role. As the AuNR-TCPP distance decreased, radiative decay rate increased, thus quantum yield (i.e., emission intensity) rised, together with the shortened fluorescence lifetime. This was again consistent with our observation when the shell thickness decreased from 34 to 22 nm. As the AuNR-TCPP distance further decreased from 22 to 8 nm, there was a simultaneous increase in the nonradiative decay rate, which caused the declining trends of quantum yield at these distances. Hence, we observed that the fluorescence enhancement factors (F) gradually decrease from the maximum 4.5 to 1.2. This was well consistent with our experimental observation when the shell thickness decreased from 22 to 8 nm (Figure 3H and Table S1, Supporting Information).

2.3. Principle of the PPi Detection

As one of the widespread metal, copper was known to be an essential trace element for both plants and animals, including humans, with a great importance in environment, industry, and biological systems. Cu^{2+} was a well-known highly efficient fluorescent quencher due to its paramagnetic properties via electron or energy transfer.[58,59] Cu^{2+} could form complexes with porphyrin molecules, resulting in the fluorescence quenching.[58,60,61] Recent research demonstrated that Cu^{2+} complexes showed strong affinity toward PPi, and could be available for design PPi sensors using displacement strategies.[33,35,41,62] Moreover, this strong association between PPi and Cu^{2+} could be further applied to determining alkaline phosphatase (ALP) with PPi as substrate.[63,64] As shown in **Figure 4**, the AuNR@SiO_2@TCPP showed red fluorescence in 4-(2-hydroxyethyl)-1-piperazineethanesulfonic acid (HEPES) buffer (10×10^{-3} M, pH 7.4), and its fluorescence intensity was significantly quenched after the addition of Cu^{2+}. The quenching effect should be related to Cu^{2+} binding with the carboxyl groups on the surface of AuNR@SiO_2@TCPP, and formation of AuNRs@SiO_2@TCPP-Cu^{2+} complexes. Owing to the stronger coordination of PPi with Cu^{2+} than carboxyl group, when PPi was added, the fluorescence intensity of the system could be recovered partially, and effectively withdraw the Cu^{2+} from the complexes of AuNR@SiO_2@TCPP-Cu^{2+}.[42] In fact, using strong affinity between PPi and Cu^{2+} complexes for detecting PPi was explicitly described in the previous reports.[30,63,65] The photographs of AuNR@SiO_2@TCPP (the inset of Figure 4) clearly showed this fluorescence turn off-on process.

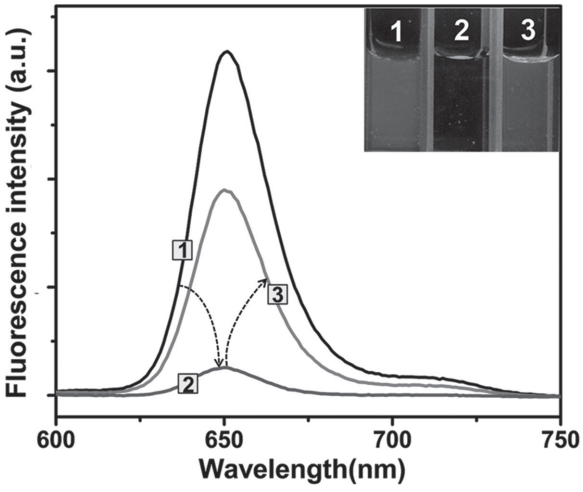

Figure 4. Fluorescence emission spectra and photographs (inset) under UV light of the 1) AuNR@SiO_2@TCPP, 2) AuNR@SiO_2@TCPP + Cu^{2+}, 3) and AuNR@SiO_2@TCPP + Cu^{2+} + PPi in 10×10^{-3} M HEPES buffer at pH 7.4.

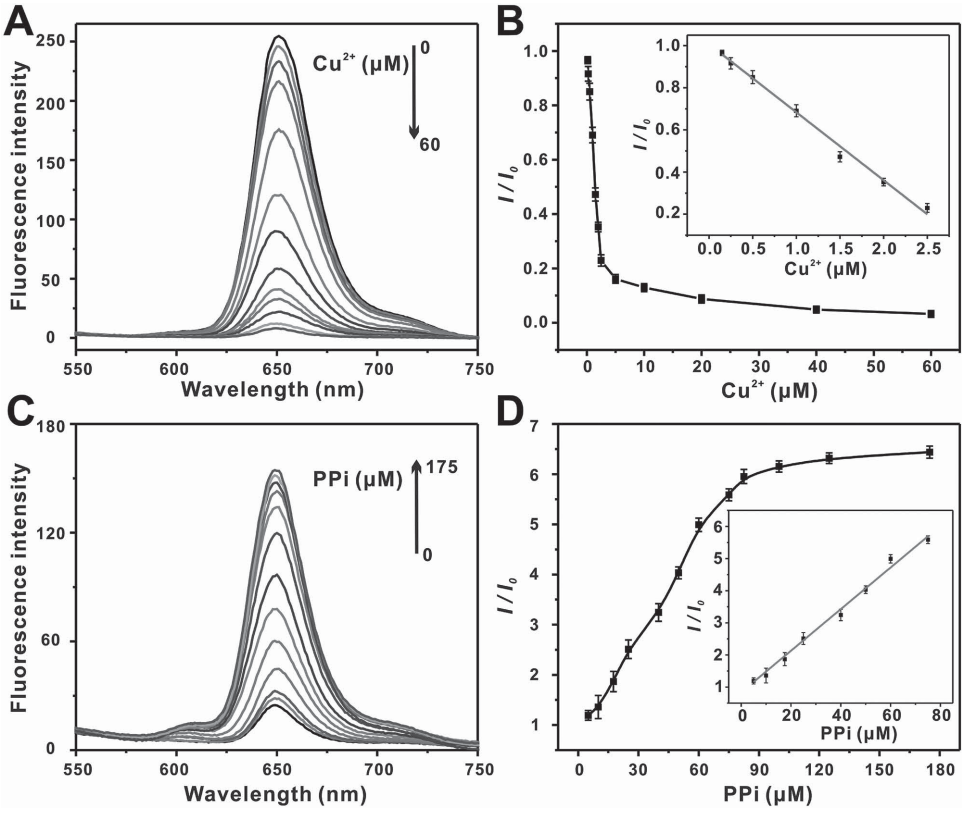

Figure 5. A) Fluorescence spectra of AuNR@SiO_2@TCPP upon addition of different concentrations of Cu^{2+} at 0, 0.15, 0.25, 0.5, 1, 1.5, 2, 2.5, 5, 10, 20, 40, and 60×10^{-6} M. B) Relative fluorescence intensity (I/I_0 at 650 nm) for AuNR@SiO_2@TCPP versus the Cu^{2+} concentrations. Inset: the fitted calibration line in the linear region of 0.15–2.5 $\times 10^{-6}$ M Cu^{2+}. C) Fluorescence spectra of the AuNR@SiO_2@TCPP-Cu^{2+} complexes upon addition of different concentrations of PPi at 0, 5, 10, 17.5, 25, 40, 50, 60, 75, 82.5, 100, 125, and 175 $\times 10^{-6}$ M PPi. D) Relative fluorescence intensity (I/I_0 at 650 nm) for AuNR@SiO_2@TCPP-Cu^{2+} (Cu^{2+}: 20×10^{-6} M) versus the PPi concentrations. Inset: the fitted calibration line in the linear region of 5–75 $\times 10^{-6}$ M PPi. Measurements were performed in 10×10^{-3} M HEPES buffer at pH 7.4.

2.4. Optimization of the Experimental Conditions for PPi Detection

For the control experiment, to understand the effect of PPi on AuNR@SiO_2@TCPP, when different concentrations of PPi were added into the same amount of AuNR@SiO_2@TCPP, the fluorescence intensities were measured. As shown in Figure S6 (Supporting Information), it was illustrated that PPi hardly affected the fluorescence ability of AuNR@SiO_2@TCPP. Therefore, a fluorescent sensor for PPi could be established through observation of the AuNR@SiO_2@TCPP-Cu^{2+} solution fluorescence. The optimization of incubation time for fluorescence quenching by Cu^{2+} was also studied. As shown in Figure S7 (Supporting Information), the fluorescence intensity decreased with the enhancement of incubation time between AuNR@SiO_2@TCPP and Cu^{2+}, and reached a plateau after 15 min, so 15 min was chosen in further experiments. The effect of the reaction time between PPi and AuNR@SiO_2@TCPP-Cu^{2+} was shown in Figure S8 (Supporting Information). The fluorescence recovery became slow until reaching a steady state at 10 min. Therefore, 10 min was selected as the optimal reaction time for PPi detection in the system.

Then, we explored the effect of Cu^{2+} concentration on the sensing system. Measurements were performed by using 0.11×10^{-9} M AuNR@SiO_2@TCPP in 10×10^{-3} M HEPES buffer at pH 7.4. **Figure 5**A showed gradual decreasing in fluorescence intensity with the increasing amount of Cu^{2+} in the range from 150×10^{-9} to 60×10^{-6} M. Additionally, the fluorescence quenched ≈90% of the initial fluorescence intensity of the unquenched AuNR@SiO_2@TCPP, when Cu^{2+} concentration was up to 20×10^{-6} M. As shown in Figure 5B, the linear correlation to the Cu^{2+} concentration was exhibited in the concentration range from 150×10^{-9} to 2.5×10^{-6} M with an R^2 of 0.994, and the limit of detection for the concentration of Cu^{2+} was calculated to be 75×10^{-9} M ($3\sigma_b/s$), which was much lower than the recent reported fluorescence methods. Besides Cu^{2+} (20×10^{-6} M), we further assessed the influence of 17 metal cations (each 40×10^{-6} M) including Na^+, K^+, Ag^+, Mg^{2+}, Ca^{2+}, Ba^{2+}, Fe^{2+}, Co^{2+}, Ni^{2+}, Zn^{2+}, Mn^{2+}, Pb^{2+}, Sr^{2+}, Cd^{2+}, Al^{3+}, Fe^{3+}, and Cr^{3+} on fluorescence of AuNR@SiO_2@TCPP in this work (see the black columns in Figure S9, Supporting Information). The fluorescence intensity ratios (I_0/I) of the AuNR@SiO_2@TCPP showed an extensive decrease in the presence of Cu^{2+}, while others had no or slight effects on the change of fluorescence intensity. Moreover, compared to other metal ions, only a

dramatic fluorescence recovery was observed by the solution composed of Cu^{2+} and AuNR@SiO_2@TCPP when introducing PPi (see the red columns in Figure S9, Supporting Information). The results indicated that this core–shell nanoprobe had excellent selectivity for Cu^{2+} over other metal ions. Thus, the concentration of 20×10^{-6} M for Cu^{2+} was chosen as the optimal conditions for the following quantitative determination.

2.5. Turn-On Fluorescent Detection of PPi

To examine the feasibility of using the AuNR@SiO_2@TCPP-Cu^{2+} as the turn-on sensing probes for PPi, different concentrations of PPi was added into 10×10^{-3} M HEPES buffer (pH 7.4) containing AuNR@SiO_2@TCPP (0.11×10^{-9} M) and Cu^{2+} (20×10^{-6} M) under the optimal conditions. As shown in Figure 5C, the fluorescence intensity of the system could be gradually recovered as the concentration of PPi increased. When the concentration of added PPi was up to 125×10^{-6} M, ≈65% of the initial fluorescence intensity of the unquenched AuNR@SiO_2@TCPP could be recovered, namely, about 6.5 times enhancement over the fluorescence intensity of AuNR@SiO_2@TCPP-Cu^{2+} (Figure 5D). A good linear fitting curve between fluorescence intensity ratios I/I_0 (where I and I_0 are the corresponding fluorescence intensities in the presence and absence of PPi, respectively) and concentration of PPi was obtained in the range of 5 10^{-6} M to 75×10^{-6} M with an R^2 of 0.993 (the inset of Figure 5D). The limit of detection (LOD) was estimated to be 820×10^{-9} M based on $3\sigma_b/s$, where σ_b was the standard deviation of the blank samples and s was the slope of the calibration curve.

To evaluate the specificity of AuNR@SiO_2@TCPP-Cu^{2+} toward PPi, the fluorescence response of AuNR@SiO_2@TCPP-Cu^{2+} toward PPi was examined in the presence of excess amounts of these anions (PO_4^{3-}, HPO_4^{2-}, $H_2PO_4^-$, Ac^-, HCO_3^-, CO_3^{2-}, NO_3^-, NO_2^-, SO_4^{2-}, SO_3^{2-}, F^-, Cl^-, Br^-, and I^-) under identical conditions (**Figure 6**). Except for $H_2PO_4^-$, HPO_4^{2-}, and PO_4^{3-}, the fluorescence intensities of AuNR@SiO2@TCPP-Cu^{2+} remained unchanged or slightly changed upon addition of 400×10^{-6} M of any of these anions. However, addition of 125×10^{-6} M of PPi resulted in a dramatic fluorescence recovery. The presence of $H_2PO_4^-$, HPO_4^{2-}, and PO_4^{3-} caused an obvious enhancement of fluorescence, because they were also able to form stable metal chelates. However, compared with the sharp increase of fluorescence by PPi and approximately four-fold lower amount of PPi, the influence of phosphate anions could be considered to be acceptable, while other anions had slight effects on the change of fluorescence intensity. These results indicated that this method had good specific for the PPi detection.

To evaluate its feasibility in real samples, this method was applied to PPi detection in tap water and in Dulbecco's modified Eagle medium (DMEM) cell medium. The average recovery and relative standard deviation (RSD) for various concentrations of PPi were generally satisfactory (Table S2, Supporting Information). The results in DMEM cell medium also verified the stability and practicability of this method in biological samples.

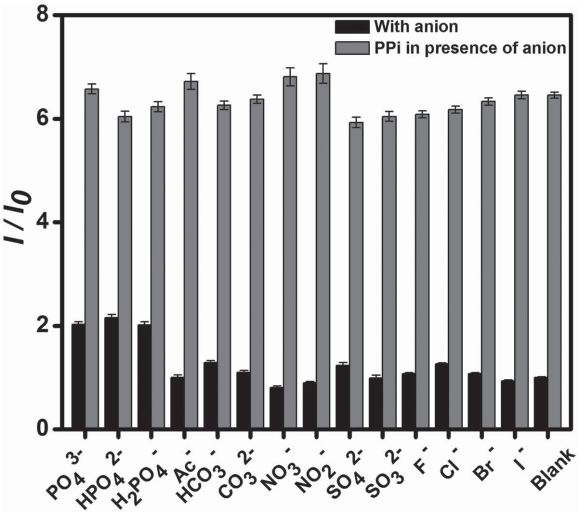

Figure 6. Fluorescence intensity ratios (where I and I_0 are the corresponding fluorescence intensities at 650 nm in the presence and absence of anions, respectively) of AuNR@SiO_2@TCPP-Cu^{2+} toward PPi in the presence of some representative analytes. Black bars represent the addition of a single analyte (400×10^{-6} M) including: PO_4^{3-}, HPO_4^{2-}, $H_2PO_4^-$, Ac^-, HCO_3^-, CO_3^{2-}, NO_3^-, NO_2^-, SO_4^{2-}, SO_3^{2-}, F^-, Cl^-, Br^-, I^-, and blank, respectively. Gray bars represent the subsequent addition of PPi (125×10^{-6} M) to the mixture. All experiments were performed in 10×10^{-3} M HEPES buffer at pH 7.4.

2.6. Cytotoxicity of AuNR@SiO_2@TCPP Nanoprobe and Imaging Cu^{2+} and PPi in Living Cells

The cytotoxicity of AuNR@SiO_2@TCPP was evaluated by the 3-(4,5-dimethylthiahizol-2-yl)-2,5-diphenyl tetrazolium bromide (MTT) viability assay of HeLa cells after incubation with NPs at different amounts for 24 h. The results of the concentration-dependent cell viability were shown in Figure S10 (Supporting Information). AuNR@SiO_2@TCPP NPs showed a high cell viability (>90%) even at high concentration (1.1×10^{-9} M), demonstrating that it was low cytotoxicity and good biocompatibility for biological imaging.

Based on the fluorescence "off" and "on" strategy of AuNR@SiO_2@TCPP nanoprobe for detection of Cu^{2+} and PPi in an order, we applied AuNR@SiO_2@TCPP nanoprobe for imaging Cu^{2+} and PPi in living cells. First, HeLa cells were incubated with 0.15×10^{-9} M AuNR@SiO_2@TCPP at 37 °C for 6 h and washed with phosphate-buffered saline (PBS) for three times to remove the free AuNR@SiO_2@TCPP prior for cell imaging. Red fluorescence of AuNR@SiO_2@TCPP in cells was observed (**Figure 7**A–C). After that, 40×10^{-6} M Cu^{2+} was introduced to the HeLa cells incubation for 1 h, the cell color was effectively quenched (Figure 7D–F). The results indicated that the AuNR@SiO_2@TCPP nanoprobe could be used for the fluorescence detection imaging of Cu^{2+} in living HeLa cells. In the addition of 250×10^{-6} M PPi, due to the higher affinity between Cu^{2+} and PPi, the observed cell color turned to red (Figure 7G–I). The results indicated that the AuNR@SiO_2@

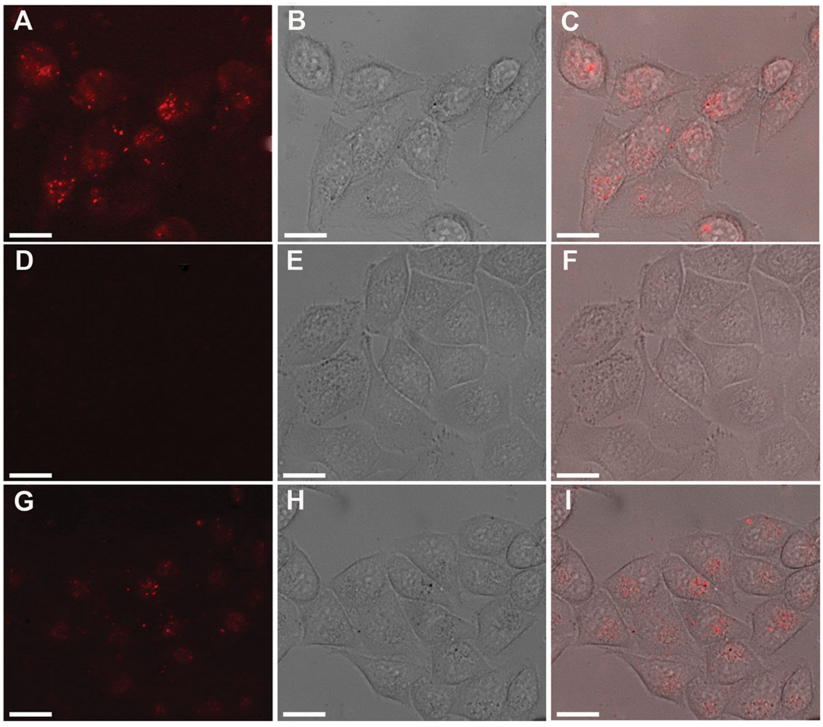

Figure 7. Fluorescence images of HeLa cells after incubation with AuNR@SiO_2@TCPP for 6 h. A) Fluorescence images, B) bright-field images, and C) merged images of the fluorescence images and bright-field images. Fluorescence images of HeLa cells after incubation with AuNR@SiO_2@TCPP for 6 h and Cu^{2+} (40×10^{-6} M) for 1 h. D) Fluorescence images, E) bright-field images, and F) merged images of the fluorescence images and bright-field images. Fluorescence images of HeLa cells after incubation with AuNR@SiO_2@TCPP for 6 h and Cu^{2+} (40×10^{-6} M) for 1 h and PPi (250×10^{-6} M) for 1 h. G) Fluorescence images, H) bright-field images, and I) merged images of the fluorescence images and bright-field images. The scale bar of all the images is 20 μm.

TCPP nanoprobe could also be applied to detect PPi in living HeLa cells.

3. Conclusion

In conclusion, we described PEF-based core–shell AuNR@SiO_2@TCPP nanostructures as an NIR fluorescent turn-on probe for sensing PPi in aqueous solutions. Through controlling the thickness of silica shell for the optimized fluorescence efficiency, AuNR@SiO_2@TCPP NPs with the shell thickness of 22 nm could obviously enhance the fluorescence intensity. The decreased average fluorescence lifetime indicated that the amplification of fluorescence was ascribed to the PEF effect. Under the optimized conditions, the proposed PEF-based nanoprobe provided an effective NIR fluorescent "turn-on" platform for detection of PPi with a detection limit of 820×10^{-9} M, and demonstrated a high selectivity in aqueous buffer. Moreover, this nanoprobe could be successfully applied to detect PPi in real samples and in living cells. Therefore, this work may not only provide a new avenue for sensing PPi but also expand the potential applications of PEF-based nanomaterials. The possibility of using the platform for other significant biomolecules assays based on plasmon-enhanced fluorescence needs more deep investigation and will be the subject of future work.

4. Experimental Section

Materials: CTAB, ascorbic acid, tetraethoxysilane (TEOS), PPi, and MTT were purchased from Sigma-Aldrich (Shanghai, China). Silver nitrate ($AgNO_3$), APTES, EDC, and NHS were obtained from Alfa Aesar (Shanghai, China). Sodium borohydride ($NaBH_4$), gold tetrachloroaurate ($HAuCl_4 \cdot 3H_2O$), sodium hydroxide (NaOH), HEPES, and $CuCl_2 \cdot 2H_2O$ were from Beijing Chemical Works. TCPP was purchased from Tokyo Chemical Industry. The HeLa human cancer of the cervix cell line, PBS, DMEM, fetal bovine serum (FBS), and penicillin–streptomycin solution (PSS) were obtained from Peking Union Medical College Hospital. All reagents used were analytical grade, and were used as received without further purification. Deionized water (18.2 MΩ) obtained from Milli-Q water purification system was used in all the experiments.

Characterization: UV–vis spectra were collected on a UV-2450 spectrometer (Shimadzu, Japan). Fluorescence spectra were collected on an RF-5301PC (Shimadzu, Japan). HR-TEM images were recorded with a JEOL 2010 transmission electron microscope at an accelerating voltage of 200 kV. The zeta potential measurements were performed using a Nano-ZS Zetasizer ZEN3600 (Malvern Instruments Ltd., UK). Time-resolved fluorescence decay curves were performed using an OB920 single-photon counting fluorometer (Edinburgh Analytical Instruments, UK) with a pulsed microsecond nitrogen lamp as excitation source. Fluorescence imaging experiments were obtained with an observer Z1 inverted fluorescence microscope (ZEISS) with blue light excitation. Confocal luminescence images were made with a Zeiss LSM700. An oil immersion objective with a numerical aperture (100×, NA 1.46) was used. The samples were excited at 405 nm.

Synthesis of AuNRs: AuNRs were synthesized in aqueous solutions using a seed-mediated growth procedure.[8] Specifically, the seed solution was first made by adding $HAuCl_4$ solution (0.25 mL, 0.01 M) into CTAB (10 mL, 0.1 M) solution and kept stirring for 1 h. Then a freshly prepared, ice-cold $NaBH_4$ solution (0.6 mL, 0.01 M) was rapidly injected into the mixture and the solution color turned from yellow to brownish-yellow under vigorous stirring for 5 min. The seed solution was then aged at room temperature until further use (for 30 min before use). The growth solution was prepared by the sequential addition of $AgNO_3$ (0.08 mL, 0.01 M), $HAuCl_4$ (0.5 mL, 0.01 M), and ascorbic acid (0.06 mL, 0.1 M) into CTAB (10 mL, 0.1 M). The growth solution was vigorously stirred for 30 s until it became colorless, the seed solution (0.01 mL) was added rapidly, and then the resultant mixture was kept overnight (for 16 h) at 27 °C. The AuNRs were then collected by washing twice at 10 000 rpm to remove excess CTAB and finally suspended in deionized water.

Synthesis of Core–Shell AuNR@SiO_2: Core–shell AuNR@SiO_2 were prepared according to the literature with slight modification and CTAB concentration was a key factor for coating different thickness of silica shell.[46] In order to ensure there was rare CTAB, the concentration of CTAB was less than 0.01×10^{-3} M. The AuNR solutions were centrifuged again at 10 000 rpm for 10 min and the precipitates were redispersed in 10 mL of water each time. The redispersed AuNR solutions were collected

and divided into six tubes of 10 mL. Then, the CTAB concentration was adjusted to 0.3, 0.4, 0.7, 0.9, 1.2, and 1.8×10^{-3} M by the addition of 0.1 M CTAB to each of the six tubes. The solutions were stored overnight to allow the CTAB bilayer to adsorb on AuNR surface evenly. Briefly, 70 µL of 0.1 M NaOH solution was added to each 10 mL of AuNR solution upon stirring for 30 min. After that, three 30 µL injections of 20% TEOS in methanol were added under gentle stirring at a 30 min interval and left to react with AuNRs for 24 h. The silica-coated AuNR suspension was separated by centrifugation and washed with water and ethanol three times. The obtained AuNR@SiO_2 NPs were redispersed in ethanol before further use.

Conjugation of TCPP with AuNR@SiO_2: The conjugation of the as-prepared core–shell AuNR@SiO_2 with TCPP was performed by amine coupling processes. First, modification of core–shell AuNR@SiO_2 with amino groups was required. Briefly, 100 µL of ammonium hydroxide (25%) was added to a 10 mL of AuNR@SiO_2 ethanol solution and stirred for 30 min. After that, 50 µL of APTES was added to the mixture under stirring at 35 °C for 3 h and quickly heated at 65 °C for 1 h. The amino-functionalized AuNR@SiO_2 NPs were collected by centrifugation and washed three times with EtOH.

Covalent binding of TCPP to the amino-functionalized AuNR@SiO_2 NPs was conducted using a modification of the standard EDC-NHS reaction. First, 0.04 mL of 1×10^{-3} M TCPP, 20 µL of 0.1 M NHS, and 20 µL of 0.1 M EDC were added into 3 mL of DMF. The solution was continuously stirred for 30 min and then 1 mL of the amino-functionalized AuNR@SiO_2 NPs was added into the mixture. The mixture was let to react 12 h under stirring. The product was collected by centrifugation and washed with ethanol and DMF to remove the unreacted TCPP molecules. Finally, the as-synthesized AuNR@SiO_2@TCPP hybrids were dispersed into DMF or HEPES buffer solution for various optical characterizations, detection, and cell experiments.

Conjugation of TCPP with SiO_2: Silica NPs were prepared by the method under low surfactant concentration and dilute TEOS conditions with NaOH as catalyst.[46] 400 µL of 0.1 M CTAB was dissolved in 50 mL of deionized water before 250 µL of 0.1 M NaOH solution was added. The mixture was stirred for 30 min and then 600 µL of 20% ethanolic TEOS was added. The solution was aged for 24 h. The as-synthesized SiO_2 were collected by centrifugation, washed with deionized water and ethanol several times, and finally redispersed in ethanol. The sample of SiO_2@TCPP NPs was prepared by the same method described above as substituting AuNR@SiO_2 with silica nanosphere.

Fluorescence Detection of Cu^{2+} and PPi: The as-prepared AuNR@SiO_2@TCPP NPs were dissolved in the HEPES buffer (10×10^{-3} M, pH 7.4) and the fluorescence intensities were recorded from 550 to 750 nm at an excitation wavelength of 419 nm. Different concentrations of Cu^{2+} solution were added into AuNR@SiO_2@TCPP in HEPES buffer (10×10^{-3} M, pH 7.4). Their fluorescence spectrum was recorded after the incubation time for 15 min.

For quantitative determination of PPi, 50.0 µL of 0.8×10^{-3} M Cu^{2+} solution was first added into 1.9 mL of AuNR@SiO_2@TCPP in HEPES buffer (10×10^{-3} M, pH 7.4) to quench the fluorescence. A certain different concentration of PPi solution was added into the above mixture. The fluorescence spectrum was recorded at the excitation wavelength of 419 nm after 10 min incubation time.

Cytotoxicity Assay by MTT Method: The cellular toxicity of the AuNR@SiO_2@TCPP NPs was evaluated using MTT cell-viability assay. HeLa cervical carcinoma cells were seeded into 96-well plates and maintained for 24 h in a humidified standard incubator with a 5% CO_2 atmosphere at 37 °C. Then, serial dilutions of AuNR@SiO_2@TCPP with known concentrations were added into cells for incubation of another 24 h. After pouring out the medium and adding 100 µL DMEM, 20 µL of 5 mg mL^{-1} MTT was added to each well and incubated for 4 h. Then, the MTT medium solution was carefully removed and replaced with 200 µL DMSO. After the plate was gently shaken for 10 min, the relative viabilities of cells were calculated with absorption values at 490 nm according to the formula.

Cellular Imaging: HeLa cells were used for fluorescence imaging. The HeLa cells were cultured in a DMEM medium supplemented with 10% FBS and 0.01% PSS in an incubator at 37 °C under a humidified atmosphere with 5% CO_2. The cells were incubated in a confocal dish to adhere for 24 h, and then the AuNR@SiO_2@TCPP NPs were added to dish for incubating another 6 h in the culture medium. After incubation, these AuNR@SiO_2@TCPP incubated cells were thoroughly washed with PBS buffer solution to remove the excess NPs and added with fresh medium. Then the cell samples were ready for fluorescence imaging measurements.

Supporting Information

Supporting Information is available from the Wiley Online Library or from the author.

Acknowledgements

L.W. and Q.S. contributed equally to this work. The authors gratefully acknowledge support from the National Natural Science Foundation of China (21475011, 21175014, 21422503, and 91027034), the National Grant of Basic Research Program of China (No. 2011CB915504), and the Fundamental Research Funds for the Central Universities.

Received: August 9, 2015
Revised: September 20, 2015
Published online: October 29, 2015

[1] J. Kirsch, C. Siltanen, Q. Zhou, A. Revzin, A. Simonian, *Chem. Soc. Rev.* **2013**, *42*, 8733.
[2] a) N. Gandra, C. Portz, L. Tian, R. Tang, B. Xu, S. Achilefu, S. Singamaneni, *Angew. Chem., Int. Ed.* **2014**, *53*, 866; b) N. Gandra, C. Portz, L. Tian, R. Tang, B. Xu, S. Achilefu, S. Singamaneni, *Angew. Chem.* **2014**, *126*, 885.
[3] M. Li, S. K. Cushing, N. Wu, *Analyst* **2015**, *140*, 386.
[4] a) H. Yuan, S. Khatua, P. Zijlstra, M. Yorulmaz, M. Orrit, *Angew. Chem., Int. Ed.* **2013**, *52*, 1217; b) H. Yuan, S. Khatua, P. Zijlstra, M. Yorulmaz, M. Orrit, *Angew. Chem.* **2013**, *125*, 1255.
[5] D. Punj, M. Mivelle, S. B. Moparthi, T. S. van Zanten, H. Rigneault, N. F. van Hulst, M. F. García-Parajó, J. Wenger, *Nat. Nanotechnol.* **2013**, *8*, 512.
[6] T. Ming, L. Zhao, Z. Yang, H. Chen, L. Sun, J. Wang, C. Yan, *Nano Lett.* **2009**, *9*, 3896.
[7] F. Tam, G. P. Goodrich, B. R. Johnson, N. J. Halas, *Nano Lett.* **2007**, *7*, 496.
[8] D. Nepal, L. F. Drummy, S. Biswas, K. Park, R. A. Vaia, *ACS Nano* **2013**, *7*, 9064.
[9] a) R. Wilson, D. V. Nicolau, *Angew. Chem., Int. Ed.* **2011**, *50*, 2151; b) R. Wilson, D. V. Nicolau, *Angew. Chem.* **2011**, *123*, 2199.
[10] V. K. Valev, B. De Clercq, C. G. Biris, X. Zheng, S. Vandendriessche, M. Hojeij, D. Denkova, Y. Jeyaram, N. C. Panoiu, Y. Ekinci, A. V. Silhanek, V. Volskiy, G. A. E. Vandenbosch, M. Ameloot, V. V. Moshchalkov, T. Verbiest, *Adv. Mater.* **2012**, *24*, 208.
[11] E. Wientjes, J. Renger, A. G. Curto, R. Cogdell, N. F. van Hulst, *Nat. Commun.* **2014**, *5*, 4236.
[12] Y. Fu, J. Zhang, J. R. Lakowicz, *J. Am. Chem. Soc.* **2010**, *132*, 5540.
[13] L. Vigderman, B. P. Khanal, E. R. Zubarev, *Adv. Mater.* **2012**, *24*, 4811.
[14] N. Gao, Y. Chen, L. Li, Z. Guan, T. Zhao, N. Zhou, P. Yuan, S. Q. Yao, Q. Xu, *J. Phys. Chem. C* **2014**, *118*, 13904.
[15] H. Hu, H. Duan, J. K. W. Yang, Z. X. Shen, *ACS Nano* **2012**, *6*, 10147.
[16] C. Wang, Y. Chen, T. Wang, Z. Ma, Z. Su, *Adv. Funct. Mater.* **2008**, *18*, 355.
[17] M. Chen, L. Shao, S. V. Kershaw, H. Yu, J. Wang, A. L. Rogach, N. Zhao, *ACS Nano* **2014**, *8*, 8208.
[18] H. Chen, Y. Xia, *Anal. Chem.* **2014**, *86*, 11062.

[19] T. Ming, H. Chen, R. Jiang, Q. Li, J. Wang, *J. Phys. Chem. Lett.* **2012**, *3*, 191.
[20] J. Liaw, H. Tsai, C. Huang, *Plasmonics* **2012**, *7*, 543.
[21] K. Sugawa, T. Tamura, H. Tahara, D. Yamaguchi, T. Akiyama, J. Otsuki, Y. Kusaka, N. Fukuda, H. Ushijima, *ACS Nano* **2013**, *7*, 9997.
[22] K. Wu, J. Zhang, S. Fan, J. Li, C. Zhang, K. Qiao, L. Qian, J. Han, J. Tang, S. Wang, *Chem. Commun.* **2015**, *51*, 141.
[23] S. H. Liu, M. Y. Han, *Adv. Funct. Mater.* **2005**, *15*, 961.
[24] H. Su, Y. Zhong, T. Ming, J. Wang, K. S. Wong, *J. Phys. Chem. C* **2012**, *116*, 9259.
[25] C. Wang, Z. Ma, T. Wang, Z. Su, *Adv. Funct. Mater.* **2006**, *16*, 1673.
[26] X. Tian, J. Guo, Y. Tian, H. Tang, W. Yang, *RSC Adv.* **2014**, *4*, 9343.
[27] T. Zhao, K. Yu, L. Li, T. Zhang, Z. Guan, N. Gao, P. Yuan, S. Li, S. Q. Yao, Q. Xu, G. Q. Xu, *ACS Appl. Mater. Interfaces* **2014**, *6*, 2700.
[28] N. Chen, K. Tang, M. Chung, S. Cheng, C. Huang, C. Chu, P. Chou, J. S. Souris, C. Chen, C. Mou, L. Lo, *Theranostics* **2014**, *4*, 798.
[29] S. K. Kim, D. H. Lee, J. Hong, J. Yoon, *Acc. Chem. Res.* **2009**, *42*, 23.
[30] S. Lee, K. K. Y. Yuen, K. A. Jolliffe, J. Yoon, *Chem. Soc. Rev.* **2015**, *44*, 1749.
[31] M. Hirose, J. Abe-Hashimoto, K. Ogura, H. Tahara, T. Ide, T. Yoshimura, *J. Cancer Res. Clin. Oncol.* **1997**, *123*, 337.
[32] S. Bhowmik, B. N. Ghosh, V. Marjomäki, K. Rissanen, *J. Am. Chem. Soc.* **2014**, *136*, 5543.
[33] Z. S. Qian, L. J. Chai, Y. Y. Huang, C. Tang, J. J. Shen, J. R. Chen, H. Feng, *Biosens. Bioelectron.* **2015**, *68*, 675.
[34] S. Kim, M. S. Eom, S. K. Kim, S. H. Seo, M. S. Han, *Chem. Commun.* **2013**, *49*, 152.
[35] X. Feng, Y. An, Z. Yao, C. Li, G. Shi, *ACS Appl. Mater. Interfaces* **2012**, *4*, 614.
[36] D. X. Li, J. F. Zhang, Y. H. Jang, Y. J. Jang, D. H. Kim, J. S. Kim, *Small* **2012**, *8*, 1442.
[37] Z. Hai, Y. Bao, Q. Miao, X. Yi, G. Liang, *Anal. Chem.* **2015**, *87*, 2678.
[38] W. Zhu, X. Huang, Z. Guo, X. Wu, H. Yu, H. Tian, *Chem. Commun.* **2012**, *48*, 1784.
[39] H. N. Lee, Z. Xu, S. K. Kim, K. M. K. Swamy, Y. Kim, S. Kim, J. Yoon, *J. Am. Chem. Soc.* **2007**, *129*, 3828.
[40] Z. Guo, S. Park, J. Yoon, I. Shin, *Chem. Soc. Rev.* **2014**, *43*, 16.
[41] S. Mirra, S. Milione, M. Strianese, C. Pellecchia, *Eur. J. Inorg. Chem.* **2015**, *2015*, 2272.
[42] H. Yoon, J. M. Lim, H. Gee, C. Lee, Y. Jeong, D. Kim, W. Jang, *J. Am. Chem. Soc.* **2014**, *136*, 1672.
[43] J. Sun, F. Yang, D. Zhao, X. Yang, *Anal. Chem.* **2014**, *86*, 7883.
[44] J. Deng, Q. Jiang, Y. Wang, L. Yang, P. Yu, L. Mao, *Anal. Chem.* **2013**, *85*, 9409.
[45] a) A. Abou-Hassan, R. Bazzi, V. Cabuil, *Angew. Chem., Int. Ed.* **2009**, *48*, 7180; b) A. Abou-Hassan, R. Bazzi, V. Cabuil, *Angew. Chem.* **2009**, *121*, 7316.
[46] N. S. Abadeer, M. R. Brennan, W. L. Wilson, C. J. Murphy, *ACS Nano* **2014**, *8*, 8392.
[47] R. Bardhan, N. K. Grady, J. R. Cole, A. Joshi, N. J. Halas, *ACS Nano* **2009**, *3*, 744.
[48] J. Liang, K. Li, G. G. Gurzadyan, X. Lu, B. Liu, *Langmuir* **2012**, *28*, 11302.
[49] L. Lu, Y. Qian, L. Wang, K. Ma, Y. Zhang, *ACS Appl. Mater. Interfaces* **2014**, *6*, 1944.
[50] W. Ni, Z. Yang, H. Chen, L. Li, J. Wang, *J. Am. Chem. Soc.* **2008**, *130*, 6692.
[51] R. Bardhan, N. K. Grady, N. J. Halas, *Small* **2008**, *4*, 1716.
[52] M. Lessard-Viger, M. Rioux, L. Rainville, D. Boudreau, *Nano Lett.* **2009**, *9*, 3066.
[53] J. R. Lakowicz, K. Ray, M. Chowdhury, H. Szmacinski, Y. Fu, J. Zhang, K. Nowaczyk, *Analyst* **2008**, *133*, 1308.
[54] R. Jiang, B. Li, C. Fang, J. Wang, *Adv. Mater.* **2014**, *26*, 5274.
[55] S. Liu, L. Huang, J. Li, C. Wang, Q. Li, H. Xu, H. Guo, Z. Meng, Z. Shi, Z. Li, *J. Phys. Chem. C* **2013**, *117*, 10636.
[56] F. Xie, M. S. Baker, E. M. Goldys, *Chem. Mater.* **2008**, *20*, 1788.
[57] J. R. Lakowicz, Y. Shen, S. D'Auria, J. Malicka, J. Fang, Z. Gryczynski, I. Gryczynski, *Anal. Biochem.* **2002**, *301*, 261.
[58] M. J. Kim, K. M. K. Swamy, K. M. Lee, A. R. Jagdale, Y. Kim, S. Kim, K. H. Yoo, J. Yoon, *Chem. Commun.* **2009**, 7215.
[59] M. Zhang, B. Ye, *Analyst* **2011**, *136*, 5139.
[60] M. Biesaga, K. Pyrzynska, M. Trojanowicz, *Talanta* **2000**, *51*, 209.
[61] Y. Weng, Y. Teng, F. Yue, Y. Zhong, B. Ye, *Inorg. Chem. Commun.* **2007**, *10*, 443.
[62] S. Liu, S. Pang, W. Na, X. Su, *Biosens. Bioelectron.* **2014**, *55*, 249.
[63] K. Xu, Z. Chen, L. Zhou, O. Zheng, X. Wu, L. Guo, B. Qiu, Z. Lin, G. Chen, *Anal. Chem.* **2015**, *87*, 816.
[64] L. Zhang, J. Zhao, M. Duan, H. Zhang, J. Jiang, R. Yu, *Anal. Chem.* **2013**, *85*, 3797.
[65] K. Selvaprakash, Y. Chen, *Biosens. Bioelectron.* **2014**, *61*, 88.